Density functional theory study of the thermodynamic and elastic properties of Ni-based superalloys

2015 J. Phys.: Condens. Matter 27 295401

(http://iopscience.iop.org/0953-8984/27/29/295401)

IOP Publishing Journal of Physics: Condensed Matter

J. Phys.: Condens. Matter **27** (2015) 295401 (15pp) doi:10.1088/0953-8984/27/29/295401

Density functional theory study of the thermodynamic and elastic properties of Ni-based superalloys

Xiaoxia Wu[1,3] **and Chongyu Wang**[1,2]

[1] Central Iron and Steel Research Institute, Beijing 100081, People's Republic of China
[2] Department of Physics, Tsinghua University, Beijing 100084, People's Republic of China
[3] School of Mathematics, Physics and Biological Engineering, Inner Mongolia University of Science and Technology, Baotou 041010, People's Republic of China

E-mail: cywang@mail.tsinghua.edu.cn

Received 29 March 2015, revised 25 May 2015
Accepted for publication 27 May 2015
Published 3 July 2015

Abstract

The thermophysical properties of Ni-based single-crystal superalloys were investigated using first-principles calculations combined with the quasiharmonic approximation. The effect of alloying elements X (X = Re, Ru, Ta, W, Mo, Cr, and Co) on the thermophysical properties of the γ-Ni and γ'-Ni_3Al phases was investigated. The calculations showed that alloying can effectively adjust the lattice misfit between the two phases, and Cr can suppress lattice misfit and may improve the creep resistance of alloys. At 0 K, doping with refractory elements leads to tetragonal shear softening of the γ-Ni phase. For γ-Ni, Re, Ru, Cr, and Co slightly increase c_{44}, while Mo, W, and Ta decrease c_{44}. Importantly, high-temperature relative hardening was found to occur close to the service temperature of the superalloy, at which Ru and Cr increase c' and Mo and W increase c_{44} of γ-Ni. For the γ'-Ni_3Al phase, all of the alloying elements except Co considerably increase c' and c_{44}. Re and W at the Al site were found to most effectively harden the γ'-Ni_3Al phase. The thermophysical and elastic properties were fully understood by analysis of the electronic structures and phonon spectra. It was found that the electronic density of states (DOS) can account for elastic hardening due to alloying. The phonon spectra along with electronic DOS analysis showed that alloying not only strengthens the first nearest neighbor Ni–X bond through additional d–d hybridization, but it is also important for stiffening the second nearest neighbor Al–X bonding through p-band filling.

Keywords: nickel-based single crystal superalloys, alloying elements, density functional theory (DFT), thermodynamic, temperature dependent elastic properties

(Some figures may appear in colour only in the online journal)

1. Introduction

Ni-based single-crystal (SC) superalloys are widely used in turbine blades in aircraft jet engines and land-based power generators because they have excellent high-temperature properties, including strength, ductility, fracture toughness, and fatigue resistance, as well as enhanced creep and oxidation resistance [1–3]. The superalloys are characterized by cubical γ' precipitate ($L1_2$, ordered face-centered cubic, Ni_3Al) embedded in the γ matrix (disordered fcc, solid solution Ni). The lattice misfit between the γ-Ni and γ'-Ni_3Al phases reflects the stability and the stress state of the two phases, and influences the microstructure and mechanical properties at the service temperature [4, 5]. Because the service temperature of superalloys is ~1000 °C, they are usually doped with platinum and refractory elements to improve the high-temperature mechanical properties and increase their lifetime [1]. Therefore, some researchers have studied the effect of alloying elements on the fundamental properties of Ni-based SC superalloys, such as generalized stacking-fault energies,

strength, and ductility, and the synergistic effect of alloying elements [6, 7]. A comprehensive understanding of alloying effects on the thermophysical and mechanical properties of each phase at finite temperature is important for the optimization of superalloys [8].

Experimentally, the coefficient of thermal expansion (CTE) of Ni, Ni_3Al, $Ni_{1-x}M_x$ (M = Cr, Mo, and Re), the β–NiAl B2 phase, and SC Ni-based superalloys at different temperatures have been reported in numerous studies [9–13]. The basic experimental data of Ni and Ni_3Al, including entropy, heat capacity, enthalpy, and Gibbs free energy, at finite temperatures were summarized by Barin [14]. The atom-probe tomography studies [7, 15, 16] showed that Re, Ru, W, Hf and Cr prefer Al sublattice of γ'-Ni_3Al phase in the ternary NiAlX alloys. The substitution of these elements in both γ-Ni and γ'-Ni_3Al phases would have measurable effects on the thermophysical properties. On the other hand, the alloying could harden the superalloys. The measurements of elastic properties of Ni-based SC superalloys using various methods indicated that the addition of refractory elements increases the elastic moduli of the matrix and precipitate [17–21]. And the elastic moduli drastically decreased with increasing temperature.

Theoretically, to calculate the structural and thermodynamic properties at finite temperature, the contribution of lattice thermal vibrations, which is the leading term of thermal effect, to the total free energy needs to be taken into account. The vibrational free energy is usually calculated by the parameterized Debye model [22–24] when efficiency is important or by the phonon model via the supercell method [22, 25–27] when accuracy is important. Shang *et al* [22] showed that the thermodynamic properties of pure Ni and Ni_3Al can be well-determined by phonon calculations, and also by the Debye model choosing suitable parameters. Using the Debye–Wang model, Kim *et al* [24] investigated alloying effects on the thermal expansion of γ-Ni and γ'-Ni_3Al. Even though the predicted CTE of several Ni–Al-based alloys from this model showed good agreement with the available experimental results, the results strongly depended on the parameter λ of the Debye–Wang model. Therefore, this model does not give reliable predictive results. The phonon spectra can be calculated from force constant determined by Parlinski–Li–Kawazoe methods [28]. This is an efficient and accurate strategy for determining phonon and thus vibrational contribution to free energy. And the combination of phonon calculation with quasi-harmonic approximation can give full density functional theory (DFT) prediction of thermophysical properties of alloys and compounds. For instance, Togo *et al* [27] calculated the thermodynamic properties of Ti_3AC_2 compounds by using such a scheme and got nice agreement between experiments and theoretical prediction.

Density functional theory has been successfully used to study the elasticity of superalloys [29–35], such as the effect of alloying elements (Ta, Mo, W, Cr, Re, Ru, Co, and Ir) on the elastic properties of the γ-Ni phase, γ'-Ni_3Al phase, and ternary and quaternary Ni-based model superalloys, and the influence of the γ'-Ni_3Al phase volume fraction on the elastic properties of the Ni[001] (100)/Ni_3Al[001] (100) model superalloys [30–32]. However, most of the calculated results are at 0 K. Generally, it is believed that 0 K DFT results can account for the high temperature elastic properties [36, 37]. However, in the current work we will show that addition of refractory elements into the γ-Ni phase can lead to high temperature ($T > 900$ K) hardening, while 0 K DFT predicts that alloying leads to tetragonal softening. Recently, Wang *et al* [26] proposed a simple quasi-static approach to calculate the elastic constants at finite temperatures using first-principles calculations. Application of this method to calculate the finite temperature elastic constants of several cubic metals and alloys [26], rare-earth intermetallic compounds [38], and doped γ-Ni phase of superalloys [23] show reasonable agreement with available experiments. However, the temperature dependence of the elastic properties of doped γ'-Ni_3Al phases has not been systematically studied.

The quasi-static approach [26] calculates the elastic constants at a given temperature through volume–temperature correspondence, where the CTE of metals and alloys is predicted by a full DFT calculation including phonon effects through the quasiharmonic approximation. Compared with the Debye models [22], the phonon calculation is parameter-free and more accurate, and thus a reliable prediction is expected. Therefore, a systematic first-principles study of the thermodynamical and thermomechanical properties of the doped γ-Ni and γ'-Ni_3Al phase of superalloys is urgently needed.

In the present work, we use DFT combined with the quasi-harmonic approximation (QHA) [21, 23] and the quasi-static approach [26, 38] to investigate the thermodynamic and temperature-dependent elastic properties of the γ-Ni and γ'-Ni_3Al phases, especially the effects of alloying elements on these fundamental properties. The rest of this paper is organized as follows: In section 2, we describe the theory and methodology for calculating the Helmholtz free energy and elastic moduli ($c_{ij}(T)$). In section 3, we briefly explain the details of the calculations with the Vienna *ab initio* simulation package (VASP), the Phonopy package, and the alloy theoretic automated toolkit (ATAT) code. In section 4, we give the results of the thermodynamic and temperature-dependent elastic properties of both the γ-Ni and γ'-Ni_3Al phases with doping alloying elements X (X = Re, Ru, Ta, W, Mo, Cr, and Co), and compare them with the available experimental data. To better understand the strengthening mechanisms of these elements, we discuss the electronic structures and phonon spectra of the γ'-Ni_3Al phase in section 5. Finally, we give a summary of the present work in section 6.

2. Theory and methodology

It is assumed that the temperature-dependence of the elastic properties is mainly caused by volume expansion. Anharmonic effects, kinetic energy contributions, and fluctuation of the microscopic stress tensors are not considered in the present work.

First, the volume change as a function of temperature $V(T)$ and CTE are calculated by the quasi-harmonic first-principles approach. To obtain the equilibrium volume at different temperatures, the Helmholtz free energy is calculated

with constant volume V and temperature T, incorporating the effects of thermal electronic excitation and thermal vibrations (phonon). For a system with volume V and temperature T, the Helmholtz free energy can be approximated as [22, 25]

$$F(V,T) = E_0(V) + F_{\rm el}(V,T) + F_{\rm vib}(V,T), \tag{1}$$

where $E_0(V)$ is the static energy at 0 K from the first-principles calculation, $F_{\rm el}$ is the thermal electronic contribution to the Helmholtz free energy, and $F_{\rm vib}$ is the vibrational free energy of the lattice atoms.

Here, $F_{\rm el}$ is defined as $F_{\rm el} = E_{\rm el} - TS_{\rm el}$, and describes the energetic contribution from thermally excited electrons at high temperatures around the Fermi level. This contribution can be ignored in systems where the energy of the band gap is larger than the thermal excitation energy ($k_{\rm B}T$, where $k_{\rm B}$ is the Boltzmann constant), such as semiconductors and insulators. However, for metallic systems, the thermal electronic contribution should be taken into account because of the non-zero electronic density at the Fermi level. The thermal electronic contribution as a function of volume V and temperature T is based on Fermi–Dirac statistics. The thermal electronic energy $E_{\rm el}$ is given by [25]

$$E_{\rm el}(T,V) = \int_{-\infty}^{\infty} n(\varepsilon,V) f(\varepsilon,T,V)\varepsilon \,{\rm d}\varepsilon - \int_{-\infty}^{\varepsilon_{\rm F}} n(\varepsilon,V)\varepsilon \,{\rm d}\varepsilon, \tag{2}$$

and the bare electronic entropy $S_{\rm el}$ is

$$S_{\rm el}(T,V) = -k_{\rm B}\int_{-\infty}^{\infty} n(\varepsilon,V)\{f(\varepsilon,T,V)\ln f(\varepsilon,T,V) + [1-f(\varepsilon,T,V)]\ln[1-f(\varepsilon,T,V)]\}{\rm d}\varepsilon, \tag{3}$$

where $n(\varepsilon,V)$, ε, and $\varepsilon_{\rm F}$ represent the electronic density of states (DOS), the energy eigenvalue, and the Fermi energy, respectively. $f(\varepsilon,T,V)$ is the Fermi–Dirac distribution function $f(\varepsilon,T,V) = 1/\left\{\exp\left[\frac{\varepsilon-\varepsilon_{\rm F}}{k_{\rm B}T}\right]+1\right\}$. The electronic heat capacity at constant volume can be determined by

$$C_V^{\rm el} = T\left(\frac{\partial S_{\rm el}}{\partial T}\right)_V. \tag{4}$$

For accuracy, $F_{\rm vib}$ is described in the present work by phonon calculations at constant volume with the following formalism [25–27, 39]:

$$F_{\rm vib}(V,T) = \frac{1}{2}\sum_{\mathbf{q},i}\hbar\omega_{\mathbf{q},i} + k_{\rm B}T\sum_{\mathbf{q},i}\ln[1-\exp(-\hbar\omega_{\mathbf{q},i}/k_{\rm B}T)], \tag{5}$$

where $\hbar$ denotes the reduced Planck constant and $\omega_{\mathbf{q},i}$ represents the phonon frequency of the ith phonon branch at the wavevector $\mathbf{q}$. The vibrational heat capacity $C_V^{\rm vib}$ and the vibrational entropy $S_{\rm vib}$ contributions from lattice vibration at constant volume are given by

$$C_V^{\rm vib} = \sum_{\mathbf{q},i} k_{\rm B}\left(\frac{\hbar\omega_{\mathbf{q},i}}{k_{\rm B}T}\right)^2 \frac{\exp(\hbar\omega_{\mathbf{q},i}/k_{\rm B}T)}{[\exp(\hbar\omega_{\mathbf{q},i}/k_{\rm B}T)-1]^2}, \tag{6}$$

and

$$S_{\rm vib} = -k_{\rm B}\sum_{\mathbf{q},i}\ln[1-\exp(-\hbar\omega_{\mathbf{q},i}/k_{\rm B}T)] + \frac{1}{T}\sum_{\mathbf{q},i}\frac{\hbar\omega_{\mathbf{q},i}}{\exp(\hbar\omega_{\mathbf{q},i}/k_{\rm B}T)-1}. \tag{7}$$

Therefore, the isochoric heat capacity and the entropy of the system can be determined by

$$C_V = C_V^{\rm el} + C_V^{\rm vib}, \tag{8}$$

$$S = S_{\rm el} + S_{\rm vib}. \tag{9}$$

In this scheme, the QHA is used to calculate the thermal properties at zero pressure. The static energy at 0 K, the vibrational free energy from the phonon DOS, and the thermal electronic contribution to the free energy are calculated for a set of volumes. The calculated equilibrium volume $V(T)$ (or inverse $T(V)$ relationship) and the isothermal bulk modulus B_T, which is the resistance to deformation by a uniform hydrostatic pressure, are determined by fitting the Helmholtz free energy–volume data to the Murnaghan equation [40]. The volume thermal expansion coefficient is given by

$$\beta(T) = \frac{1}{V}\left(\frac{\partial V}{\partial T}\right)_P, \tag{10}$$

where V is the equilibrium volume at temperature T.

Second, the isothermal elastic constants c_{ij}^T are calculated. For a cubic solid, the three independent elastic constants c_{11}^T, c_{12}^T, and c_{44}^T completely describe the elastic behavior of the system. Calculation of the elastic constants at finite temperatures is quite cumbersome because it involves calculation of the second derivatives of $F_{\rm vib}$ and $F_{\rm el}$. However, plenty of experimental observations [41, 42] have verified that the temperature dependence of the elastic constants mainly results from thermal expansion. Hence, the contributions of $F_{\rm vib}$ and $F_{\rm el}$ to these second derivatives can be ignored in the calculation of the isothermal elastic constants. At a given volume V and temperature T, the applied strain configurations and the corresponding energy density–strain relationships are as follows [30–32]: $e = (0,0,0,\delta,\delta,\delta)$ with $\Delta F/V_0 = \Delta E_0/V_0 = 3/2c_{44}^T\delta^2$, and $e = (\delta,\delta,(1+\delta)^{-2}-1,0,0,0)$ with $\Delta F/V_0 = \Delta E_0/V_0 = 6c'\delta^2 + O(\delta^3)$. A set of distortions with the parameters varying from −0.03 to 0.03 in steps of 0.005 are used to fit the elastic constants. The shear constants are determined by $c' = 1/2(c_{11}^T - c_{12}^T)$. In addition, the elastic constants c_{11}^T and c_{12}^T are obtained by combining the isothermal bulk modulus $B_T = (c_{11}^T + 2c_{12}^T)/3$ and the tetragonal shear constant c'.

Finally, most of the experimental elastic constants are reported as isentropic elastic constants, because the measurements were conducted on an adiabatic system in which the elastic wave travels faster than the rate of heat conduction. Therefore, the isothermal elastic constants must be converted to the isentropic elastic constants to compare them with the available experimental results. According to the approximation by Davies [43], the isothermal and isentropic elastic constants can be determined by

Table 1. Vibrational contributions to the Helmholtz free energy for the different supercell size at 300, 1000, and 1600 K.

	Ni (eV/4 atoms)			$Ni_{31}Re$ (eV/32 atoms)		
Supercell size	300 K	1000 K	1600 K	300 K	1000 K	1600 K
2 × 2 × 2 (32)	− 0.015	− 1.335	− 2.917	− 0.145	− 10.750	− 23.454
3 × 3 × 3 (108)	− 0.015	− 1.333	− 2.914	—	—	—
4 × 4 × 4 (256)	− 0.012	− 1.324	− 2.900	− 0.134	− 10.715	− 23.400
	Ni_3Al (eV/4 atoms)			$Ni_{24}Al_7Re$ (eV/32 atoms)		
Supercell size	300 K	1000 K	1600 K	300 K	1000 K	1600 K
2 × 2 × 2 (32)	0.000	− 1.281	− 2.845	0.023	− 10.242	− 22.646
3 × 3 × 3 (108)	0.002	− 1.283	− 2.835	—	—	—
4 × 4 × 4 (256)	0.007	− 1.262	− 2.799	0.047	− 10.050	− 22.266

$$c_{ij}^S(T,V) = c_{ij}^T(T,V) + \frac{TV\lambda_i\lambda_j}{C_V} \quad \left(\lambda_i = -\sum_j \alpha_j c_{ij}^T(T,V)\right), \tag{11}$$

where α_j ($j = 1, 2, \ldots, 6$) is the linear thermal expansion tensor.

For cubic materials, equation (11) can be simplified as

$$\begin{aligned} c_{44}^S &= c_{44}^T, \\ c_{11}^S &= c_{11}^T + \Delta, \\ c_{12}^S &= c_{12}^T + \Delta, \end{aligned} \tag{12}$$

$$B_S = B_T C_P / C_V = B_T + \Delta, \tag{13}$$

where B_S and C_P are the isentropic bulk modulus and the heat capacity at constant pressure, respectively. C_P and Δ are given by

$$C_P = C_V + \beta^2 B_T T V, \tag{14}$$

$$\Delta = \frac{TV(\beta B_T)^2}{C_V}. \tag{15}$$

with the linear thermal expansion tensor is $\alpha_1 = \alpha_2 = \alpha_3 = \alpha = \beta/3$ and $\alpha_4 = \alpha_5 = \alpha_6 = 0$ in Voigt notation.

3. Computational details

The static energy and the thermal electronic contribution to the Helmholtz free energy of the γ-Ni and γ'-Ni_3Al phases at different volumes were calculated within the framework of DFT using VASP [44] and the ATAT code [45]. 32-atom 2 × 2 × 2 supercells were used for Ni and Ni_3Al with a single alloying atom X in the supercell, e.g. $Ni_{31}X$ and $Ni_{24}Al_7X$ (X = Re, Ru, Ta, W, Mo, Cr, and Co). Since the atomic percentage of alloying elements such as W, Mo and Re is usually smaller than ~3 at.%, namely, the alloying is in a dilute limit. Therefore, this 2 × 2 × 2 supercell with one impurity X is a reasonable approximation in the investigation of alloying effect of superalloys. According to recent experiments and density functional theory calculations [7, 46, 47], the alloying elements Re, Ru, Ta, W and Mo usually prefer the Al site in the γ'-Ni_3Al phase, and Co and Cr usually randomly occupy the Ni and Al sites. Therefore, in our calculation, we just considered the case of Al site occupation.

For the DFT calculations, the projector augmented wave method [48, 49] and the generalized gradient approximation of Perdew, Burke, and Ernzerhof [50] were used. The atomic arrangements were relaxed using the Methfessel–Paxton method with a smearing width of 0.07 eV [51], and an 8 × 8 × 8 k-point mesh was chosen according to the Monkhorst–Pack scheme [52]. To ensure convergence of the calculations, a plane-wave cutoff energy of 500 eV and an energy convergence criterion of 10^{-8} eV for self-consistency were used for all of the calculations.

The spin-polarized calculation was conducted in the γ-Ni phase because of the ferromagnetism of Ni under ambient conditions. However, the magnetic contribution was ignored for γ'-Ni_3Al because Ni_3Al is a weak ferromagnet with a Curie temperature T_C of ~41 K and a magnetic moment of ~0.23 μ_B [53]. Numerous DFT investigation show that the spin polarized and non-spin polarized calculation give almost the same lattice constants and bulk modulus for Ni_3Al [6, 7, 54]. Therefore, we believe that the magnetism would have very small effect on the thermodynamic and elastic properties of Ni_3Al at high temperature. All atomic positions in the supercell were relaxed to equilibrium until the quantum-mechanical Hellmann–Feynman force was less than 10^{-4} eV Å^{-1} per atom. The thermal electronic contribution was calculated within the one-electron and temperature-independent band approximations by the Felec code in ATAT, in which the Fermi–Dirac function was chosen for the smearing of the k-point grid.

The vibrational free energies were calculated by the supercell approach [27]. The real-space force constants of the supercells were calculated using the Parlinski–Li–Kawazoe method [28] with a finite displacement of 0.01 Å as implemented in VASP, and the phonon frequencies were calculated from the force constants using the Phonopy code [39]. To evaluate the supercell size dependency of the phonon property, the vibrational free energies were compared for the different supercells and temperatures, as shown in table 1. From these results, the energy differences among different supercell sizes were very small with changing temperature. For computational efficiency and without loss of generality, a 2 × 2 × 2 supercell with 32 atoms was chosen to calculate the thermal properties.

The Helmholtz free energies were calculated at 11 volume points every 50 K from 0 to 1600 K, which is close to the melting point of pure Ni (1728 K) and Ni_3Al (1663 K). The Helmholtz free energies were fitted to the Murnaghan

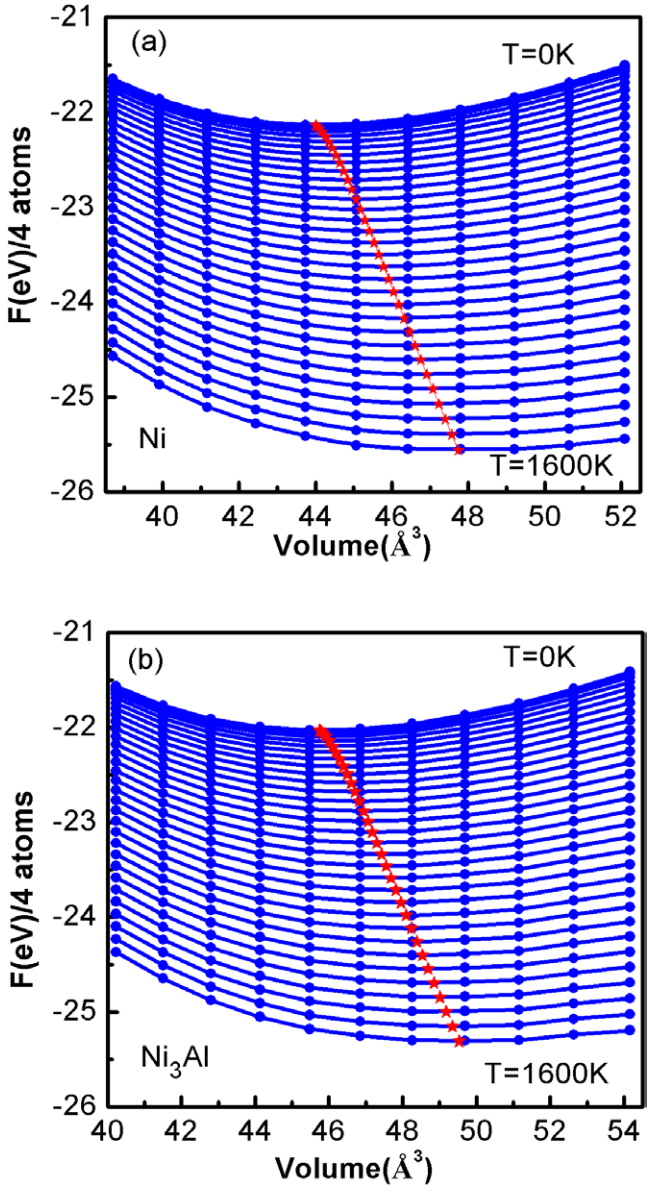

Figure 1. Helmholtz free energies $F(V, T)$ as a function of volume for Ni and Ni_3Al. The blue circles are $F(V, T)$ calculated at the volume points every 50 K between 0 and 1600 K. The blue solid curves show the fitted thermodynamic functions from the Murnaghan equation. The minimum values of the fitted thermodynamic functions at different temperatures are shown by the red five-pointed stars. The red dashed curves passing through the five-pointed stars are guides for the eye.

equation of state to determine the equilibrium volume (V_0) and bulk modulus (B_T) at finite temperatures. The calculated Helmholtz free energies for γ-Ni and γ'-Ni_3Al are shown in figure 1. The volume thermal expansion coefficient was obtained by numerical differentiation ($\partial V/\partial T$).

4. Results

4.1. Lattice misfit

The lattice misfit between two phases is crucially important for Ni-based superalloys because the rupture and creep of superalloys at high temperature are strongly correlated with the misfit strain. The highest creep strength of the Ni–Al–Cr alloy corresponds to zero lattice misfit [55]. That is, the smaller the lattice misfit strain in superalloys, the better the rupture and creep strength at high temperature. Moreover, the lattice misfit modulates the growth and accumulation of the γ'-Ni_3Al phase, and the thermal stability of the γ'-Ni_3Al phase is very important for the high-temperature strength of Ni-based superalloys. Therefore, tailoring the lattice misfit by alloying could be an efficient way to improve the high-temperature strength of this class of superalloy.

The lattice misfit is defined as $\delta = 2(a_{\gamma'} - a_\gamma)/(a_{\gamma'} + a_\gamma)$, where a_γ and $a_{\gamma'}$ are the lattice parameters of the γ-Ni and γ'-Ni_3Al phase, respectively. The misfit δ depends on the composition of both phases and the temperature. The calculated values of the lattice parameters of Ni and Ni_3Al are 3.526 and 3.574 Å at 0 K, which agrees very well with the experimental values of 3.52 and 3.57 Å, respectively. The lattice misfit is ~1.2% at 0 K, which is in good agreement with the experimental value of 1.41%. Hence, the lattice misfit values of alloys with different doping elements calculated at various temperatures (table 2) are expected to be quite accurate.

From table 2, all of the alloying elements considered here decrease the lattice misfit by over 10% ($(\delta_{\text{undoped}} - \delta_{\text{doped}})/\delta_{\text{undoped}}$) at 0 K when they are doped in both phases, which is in agreement with a previous study [30]. In addition, all of the elements except Co further suppress the misfit at high temperature. Among these elements, Cr is the most effective in decreasing lattice misfit. Doping a small amount of Cr (~3 at.%) can decrease δ by ~16% at 0 K, and this percentage decrease will be up to ~18% at ~1200 K, which is very close to the working temperature of superalloys. Moreover, the refractory elements Re, Ru, and Mo also show a large decrease in δ of up to ~15% at ~1500 K. The main reason for the decrease of δ is that alloying changes the equilibrium lattice parameters and thermal expansion coefficients of the two phases (see section 4.2). Doping the γ' phase with Cr considerably decreases the lattice parameter because Cr has a smaller atomic radius than the host Al atom. However, the lattice parameters of the γ-Ni phase doped with Cr slightly increase. The changes of the lattice parameters because of Cr addition hold at high temperature, and hence it is effective to suppress the lattice misfit.

Addition of refractory elements, such as Re, Ru, W, and Mo, considerably increase the lattice parameters of both the γ-Ni and γ'-Ni_3Al phases. Here, it can be speculated that doping the γ-Ni phase with an appropriate amount of a refractory element and adding Cr into the γ'-Ni_3Al phase could produce a two-phase superalloy with zero interface misfit. Therefore, it is expected that co-doping with different elements in the different phases can further decrease lattice misfit, and thus improve the high temperature creep strength of superalloys.

The change of lattice misfit with temperature is because of the variation of the two-phase equilibrium and the difference in the thermal expansion coefficients of the two phases at high temperature [5]. The effect of alloying on thermal expansion will be discussed in the following subsection.

Table 2. Lattice misfit of γ-Ni and γ'-Ni_3Al phases with and without doping elements at different temperatures.

	Lattice misfit δ (%)							
T (K)	Undoped	Re	Ru	Co	Cr	Mo	W	Ta
0	1.225	1.081	1.063	1.089	1.024	1.085	1.087	1.073
300	1.211	1.062	1.056	1.082	1.008	1.077	1.077	1.066
600	1.202	1.044	1.054	1.075	0.988	1.068	1.066	1.056
900	1.188	1.021	1.045	1.064	0.97	1.051	1.052	1.041
1200	1.171	0.997	1.023	1.051	0.957	1.023	1.038	1.018
1500	1.152	0.973	0.978	1.044	0.956	0.981	1.03	0.984

4.2. Linear thermal expansion coefficient and bulk modulus

The linear CTE values (α) of both the γ-Ni and γ'-Ni_3Al phases and the alloys doped with alloying elements X (X = Re, Ru, Ta, W, Mo, Cr, and Co) at finite temperatures are shown in figure 2. The linear CTE values of the undoped γ-Ni and γ'-Ni_3Al phases are compared with the experimental data [10, 56] and other theoretical results [22] in figures 2(a) and (b). The calculated CTE values of both the γ-Ni and γ'-Ni_3Al phases show good agreement with the experimental results [10, 56], except the CTE of the γ-Ni phase at its magnetic Curie temperature (figure 2(a)), which is because of the magnetic order–disorder phase transition [57]. For superalloys, the working temperature is far above the Curie temperature of the two phases. Thus, the magnetic contributions are not considered in the following discussion.

The linear CTE values of the γ-Ni and γ'-Ni_3Al phases with various alloying elements at finite temperatures are shown in figures 2(c) and (d). For the γ-Ni phase (figure 2(c)), as the temperature increases, the CTE rapidly increases up to ~350 K for all of the alloying elements, and then the CTE gradually increases with further increasing temperature. For the doped γ'-Ni_3Al phases, the threshold value is ~400 K (figure 2(d)). Almost all of the alloying elements considered decrease the CTE values of both the γ-Ni and γ'-Ni_3Al phases, except for the addition of Ru in γ-Ni and Co in γ'-Ni_3Al, which increase the CTE when $T > 1300$ K. This shows that the addition of alloying elements can effectively suppress the expansion of the system at finite temperature. Furthermore, from figure 2(c), Re and W have the strongest effect on the γ-Ni phase, and Mo is very effective at low temperature but its effect decreases for $T > 1100$ K. The effect of Cr is not significant at low temperature, but becomes stronger at high temperature. For the γ'-Ni_3Al phase, Re, W, and Mo are the most effective alloying elements (see figure 2(d)). The effect of Co is the weakest in both the γ-Ni and γ'-Ni_3Al phase.

Comparing figures 2(c) and (d), Ni_3Al has a smaller CTE than γ-Ni and almost all of the alloying elements decrease the CTE. Therefore, the lattice misfit significantly decreases with increasing temperature. The refractory elements (W, Re, Mo, and Ru) prefer the γ-Ni phase [1], and Cr has considerable solubility in the γ'-Ni_3Al phase of the quaternary superalloy [47]. This indicates that the synergistic effect of co-doping can effectively decrease lattice misfit, and consequently improve the high temperature creep strength of superalloys.

The isothermal bulk moduli (B_T) of the superalloys were obtained by fitting the total free energy–volume data to the Murnaghan equation. To compare the calculated results with the available experimental results, the isentropic bulk moduli (B_S) of both the undoped and doped phases were calculated using equation (13), and are shown in figure 3. The overall trend is that B_S decreases with increasing temperature and the slope of the $B_S(T)$ curves are almost zero at around 0 K and constant at higher temperature. Compared with the experimental results [58, 59], the calculated B_S values of the undoped γ-Ni and γ'-Ni_3Al phases are generally less than the experimental values. However, the predicted B_S values from the current calculations are very close to those obtained by other theoretical methods [22] (see figure 3(a)). Alloying considerably increases the bulk moduli of both phases. For the γ-Ni phase, the addition of alloying elements (except Cr) increase B_S at lower temperatures ($T < 400$ K), and the addition of Ru, Mo, and Ta decrease B_S of the system when the temperature is higher than 700, 1200, and 1250 K, respectively. The addition of Re and W into the γ-Ni phase can increase B_S in the temperature range 0–1600 K. Meanwhile, for the γ'-Ni_3Al phase, the addition of all of the alloying elements except Co increase B_S when $T > 1250$ K (see figure 3(c)). Among the alloying elements, the effects of Re and W are the most apparent, followed by Mo. Thus, alloying can improve the incompressibility of the γ-Ni and γ'-Ni_3Al phases, and Re and W are the most promising alloying elements.

From the above discussion on the CTE and bulk modulus, the addition of alloying elements can effectively suppress the deformation of the γ-Ni and γ'-Ni_3Al phases. The effect of Re and W are the most obvious, which is consistent with the fact that Re and W are important alloying elements to improve the mechanical properties of Ni-based superalloys [1].

4.3. Entropy and heat capacity

In thermodynamical modeling, entropy (S) is an important thermodynamic quantity, which mainly includes the bare electronic entropy (S_{el}) and the vibrational entropy S_{vib}. According to equations (3), (7), and (9), the entropies of the γ-Ni and γ'-Ni_3Al phases were calculated, and the curves of S are plotted as a function of temperature in figure 4. The entropy of the undoped γ-Ni phase is consistent with the other calculated result [22] for the whole temperature range, although it is less than the experimental value [14] at high temperatures, as shown in figure 4(a). The entropy of the doped γ-Ni phase is shown in figure 4(c), and compared with the undoped γ-Ni phase. The addition of alloying elements only slightly affects

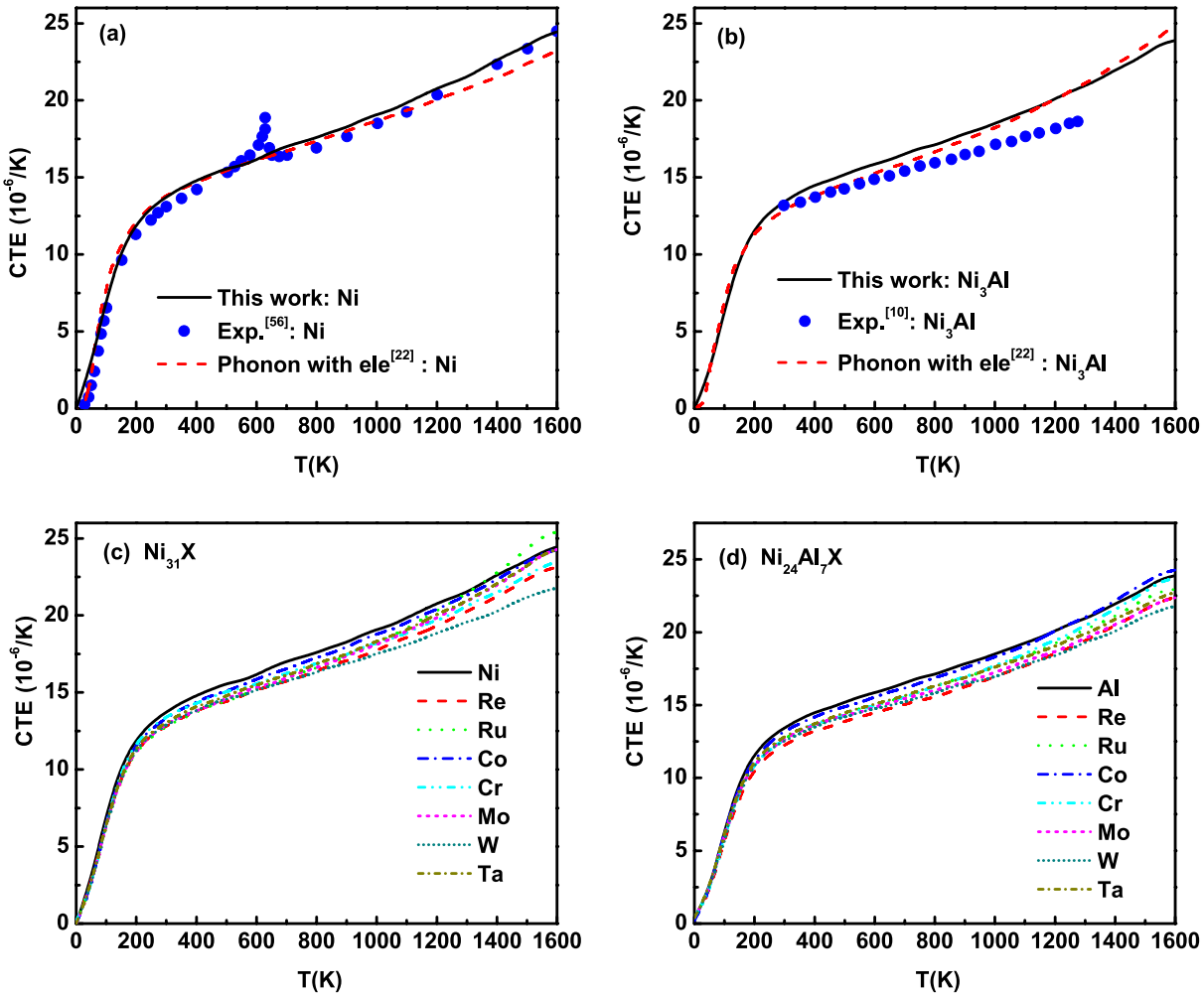

Figure 2. Linear coefficient of thermal expansion (CTE) as a function of temperature: (a) Ni, (b) Ni_3Al, (c) $Ni_{31}X$, and (d) $Ni_{24}Al_7X$. The experimental and calculated values for Ni [22, 56] and Ni_3Al [10, 22] are also shown in (a) and (b), respectively.

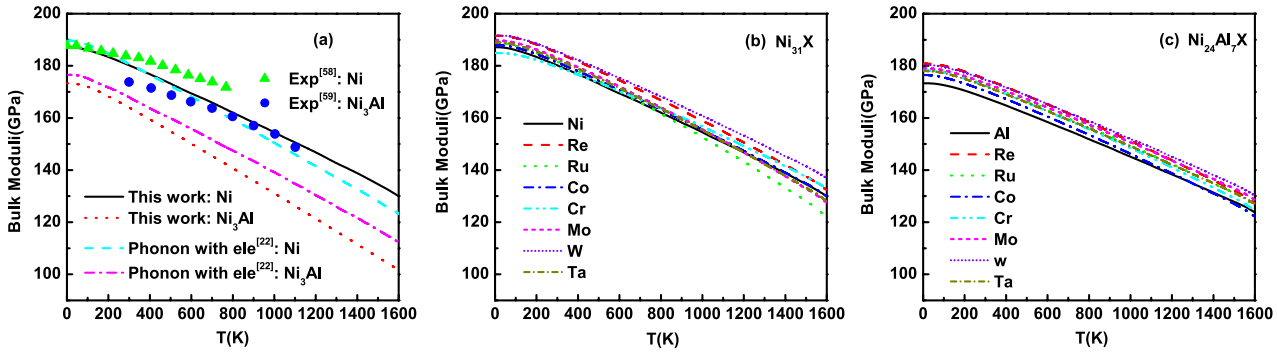

Figure 3. Isentropic bulk modulus B_S as a function of temperature for (a) Ni and Ni_3Al, (b) $Ni_{31}X$, and (c) $Ni_{24}Al_7X$. The experimental and calculated values for Ni and Ni_3Al [22, 58, 59] are also shown in (a).

the system entropy, where the differences are less than 1%. S of the undoped and doped γ'-Ni_3Al phases are shown in figures 4(b) and (d), respectively. From figure 4(b), our calculated results are consistent with both the experimental [14] and other calculated [22] values for the whole temperature range. The addition of alloying elements only slightly affects S of the γ'-Ni_3Al phase at low temperature, while the addition of Co increases S and the other elements decrease S at high temperature, as shown in figure 4(d).

The heat capacity C measures the heat energy required to change a substance's temperature by 1 K. For a system, there are the isochoric heat capacity C_V and the heat capacity at constant pressure C_P. With the aid of the calculated electronic and vibrational DOS, the isochoric heat capacity C_V can be obtained by equation (8). Then, the heat capacity at constant pressure C_P is estimated by equation (14). The estimated C_V and C_P at zero pressure are plotted in figure 5, which includes the heat capacities of Ni, Ni_3Al, $Ni_{31}X$, and $Ni_{24}Al_7X$ (X = Re,

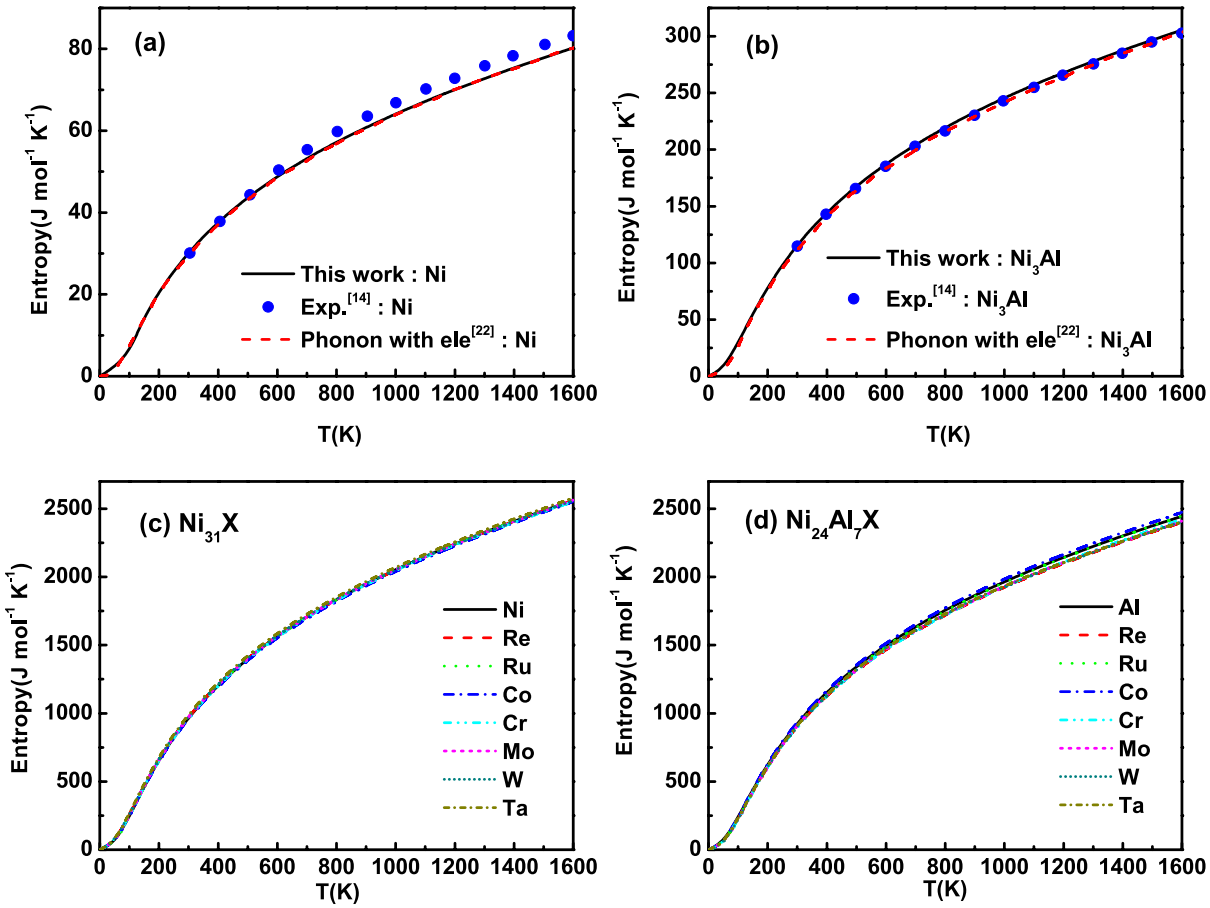

Figure 4. Entropy S as a function of temperature T for (a) Ni, (b) Ni_3Al, (c) $Ni_{31}X$, and (d) $Ni_{24}Al_7X$. The experimental and calculated results [14, 22] are shown for Ni and Ni_3Al in (a) and (b), respectively. Note that the units of entropy are per mole of the formula unit.

Ru, Ta, W, Mo, Cr, and Co) from 0 to 1600 K. From figure 5, C_V and C_P rapidly increase for $T < 300$ K, then the rate of increase decreases, and finally C_V is almost constant while C_P gradually increases with increasing T. This is reasonable because C_V conforms to a classical equipartition law $C_V = 3Nk_B$ at high temperature, where N is the number of atoms in the system, and C_P is proportional to T because of anharmonicity, as defined by equation (14). C_V and C_P of undoped Ni and Ni_3Al are plotted as a function of temperature in figures 5(a) and (b), respectively, including the experimental data [14, 56] and the other calculated results [22]. The C_P of the undoped Ni is in good agreement with the experimental value and the other calculated result. The anomaly of C_P in the experimental curve is because of the magnetic phase transition, as mentioned in section 4.2. C_P of the undoped γ'-Ni_3Al phase is slightly less than the other calculated values when $T > 800$ K [22], but agrees well with the experimental result. Furthermore, C_P of the doped γ-Ni and γ'-Ni_3Al phases are plotted as a function of temperature in figures 5(c) and (d). All of the alloying elements slightly decrease C_P of the γ-Ni phase, because the atomic fractions of the dopants are too small to have a significant effect. However, the effect of alloying elements on C_P of the γ'-Ni_3Al phase is different. The addition of Ru, Co, and Cr increase C_P of the system when $T > 500$ K, $T > 1100$ K, and throughout the whole temperature range considered, respectively. The other alloying elements considered decrease C_P in the range 0–1600 K, especially Re and W.

4.4. Temperature-dependent elastic properties

The temperature-dependent isothermal elastic constants were calculated by the total energy–strain approach at every 100 K between 0 and 1600 K, and then converted to the isentropic elastic constants (c_{ij}^S) using equation (12). The temperature dependence of the isentropic elastic constants of the undoped and doped γ-Ni and γ'-Ni_3Al phases are summarized in figure 6. As expected, the c_{ij}^S values monotonically decreases with increasing temperature for both the γ-Ni and γ'-Ni_3Al phases. The thermal expansion weakens the bonding between atoms, softening the elastic modulus at high temperature. The isentropic elastic constants satisfy the mechanical stability conditions $c_{11} - c_{12} > 0$, $c_{11} > 0$, and $c_{44} > 0$ in the range 0–1600 K for both systems. This indicates that the alloying elements do not break the dynamical stability of the systems at finite temperature.

Firstly, the isentropic elastic constants c_{11}^S, c_{12}^S, and c_{44}^S of the γ-Ni and γ'-Ni_3Al phases at finite temperatures are compared with the available experimental results and other theoretical calculations in figures 6(a) and (b). The calculated elastic constants are in good agreement with the experimental data [58,

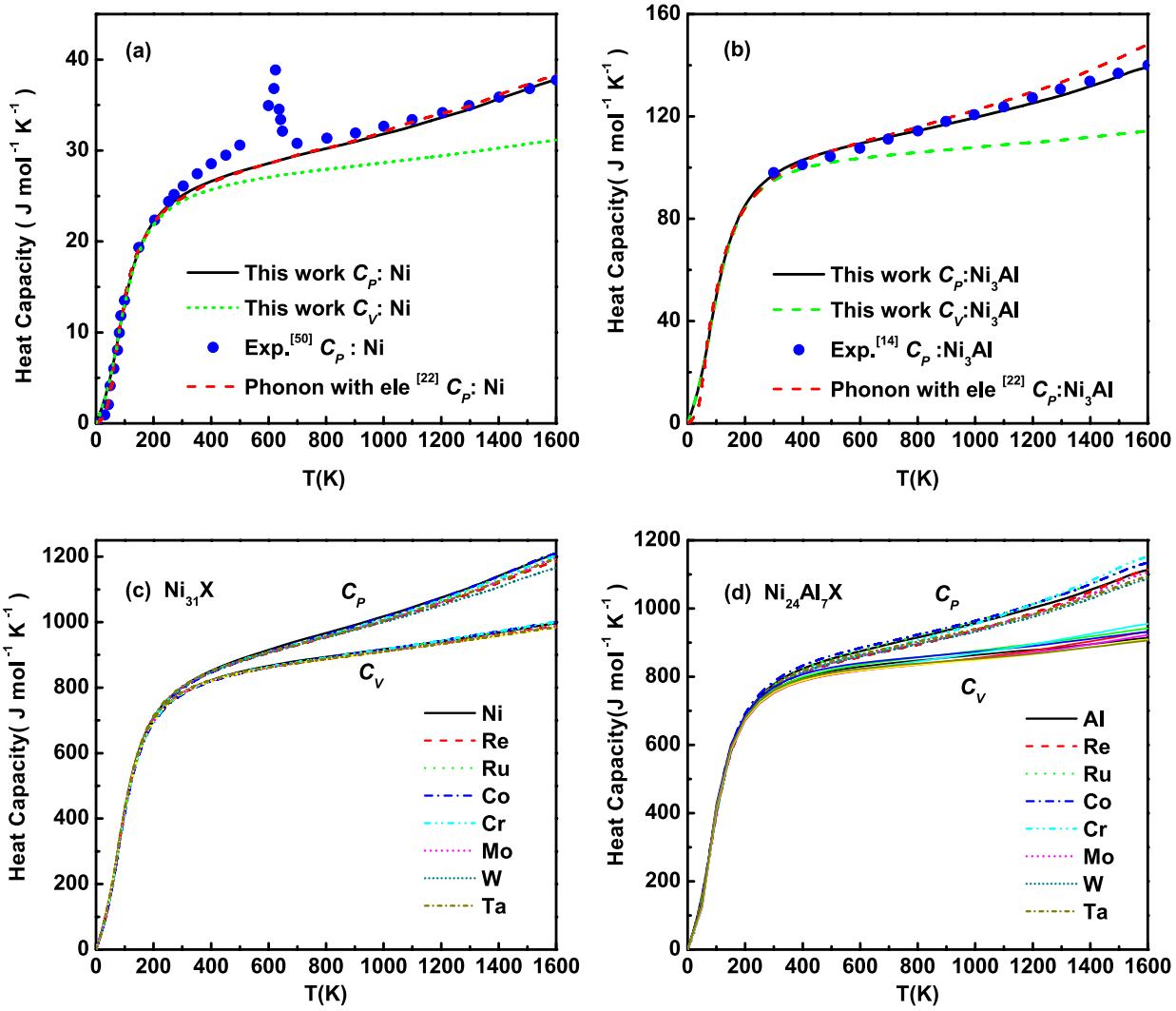

Figure 5. Isochoric heat capacity C_V and heat capacity at constant pressure C_P as a function of temperature for (a) Ni, (b) Ni_3Al, (c) $Ni_{31}X$, and (d) $Ni_{24}Al_7X$. The experimental and calculated C_P for Ni and Ni_3Al [14, 22, 56] are shown in (a) and (b), respectively. Note that the units for heat capacity are per mole of the formula unit.

59] and other theoretical calculations [26]. This is a useful test of the accuracy of the calculations. Secondly, the calculated results for the isentropic elastic constants of the doped γ-Ni and γ'-Ni_3Al phases are shown in figures 6(c) and (d). The tetragonal shear modulus $c' = 1/2(c_{11}^T - c_{12}^T) = 1/2(c_{11}^S - c_{12}^S)$ is also shown in the figures. From the viewpoint of application, the two cubic shear moduli c' and c_{44}, which are the shear resistance across the (1 0 0) plane in the <0 1 0> direction and across the (1 1 0) plane in the <1–10> direction, are the basic mechanical characteristics of superalloys. Alloying of the γ-Ni phase with element X (X = Re, Ru, Ta, W, Mo, Cr, and Co) generally softens the lattice under tetragonal deformation, except for Co, which slightly increases c'. The alloying elements Re, Ru, Cr, and Co slightly harden the rhombohedral shear modulus c_{44}, while Mo, W, and Ta decrease c_{44} of dilute Ni–X alloys. Among these elements, Ta significantly decreases c' and c_{44}. The temperature dependence of c' and c_{44} are affected by alloying, where doping of Ru and Cr into the γ-Ni phase will make the c' of $Ni_{31}X$ alloys less sensitive to temperature. Namely, the c' values of the $Ni_{31}Ru$ and $Ni_{31}Cr$ alloys are larger than that of pure Ni for $T > 800$ K and $T > 1300$ K, respectively, even though they soften c' at lower temperatures. A similar temperature dependence of c_{44} was also observed for the $Ni_{31}X$ alloys. The addition of Mo and W decrease c_{44} for $T < 900$ K, but increase c_{44} for $T > 900$ K. These results are basically consistent with those in [23]. For the γ'-Ni_3Al phase, all of the alloying elements except for Co considerably increase c' and c_{44} at finite temperature, as shown in figure 6(d). In other words, the addition of alloying elements can inhibit shear deformations across the (1 0 0) plane in the <0 1 0> direction and across the (1 1 0) plane in the <1–10> direction, which is consistent with a previous study at zero temperature [30]. Alloying does not considerably change the temperature dependence of the two cubic shear moduli, and Re and W at Al sites were found to be the most effective in hardening the γ'-Ni_3Al phase.

5. Discussion

To understand the basic electronic basis of the alloying effect on the thermophysical and elastic properties of superalloys,

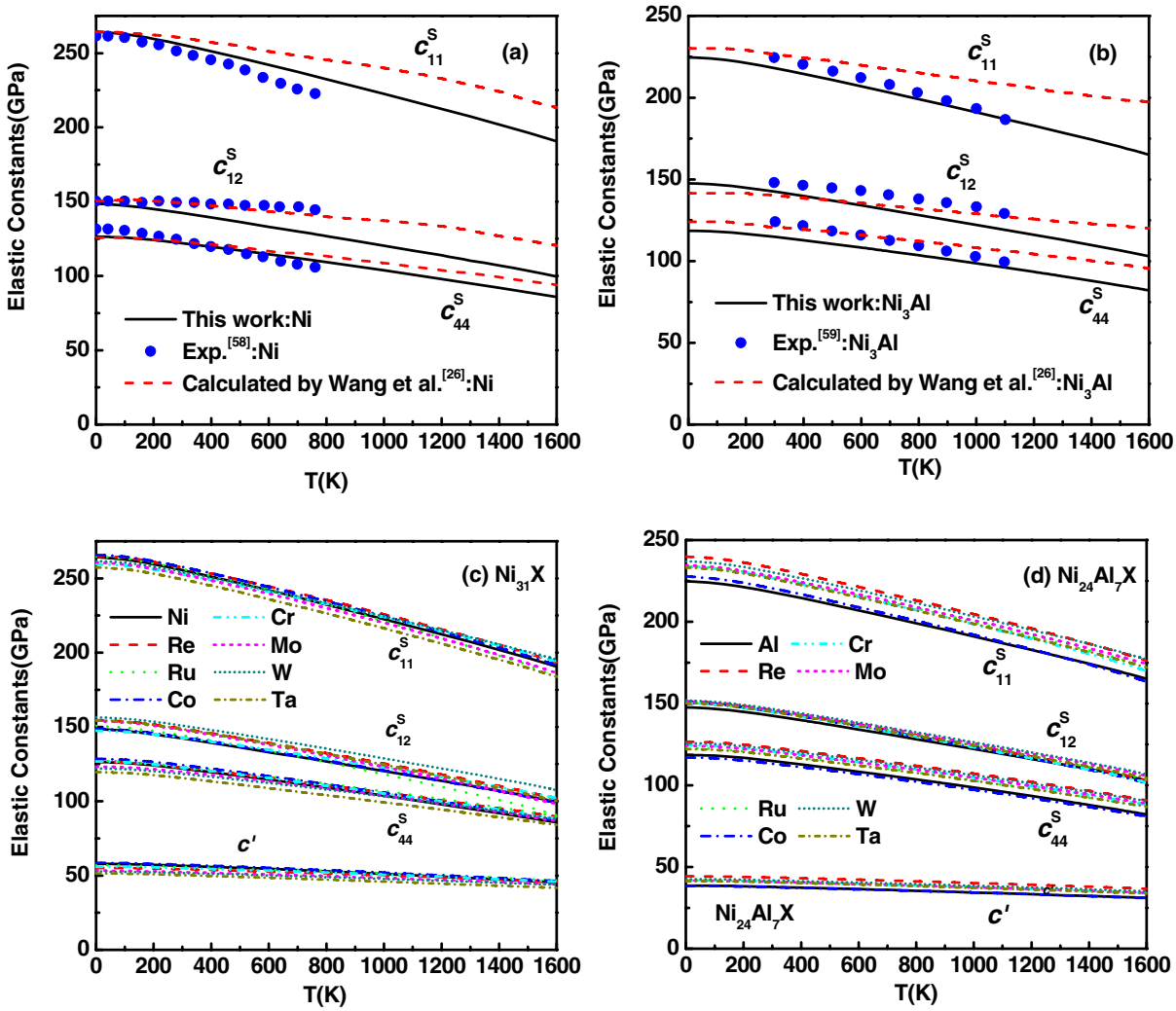

Figure 6. Calculated isentropic elastic constants as a function of temperature for (a) Ni, (b) Ni_3Al, (c) $Ni_{31}X$, and (d) $Ni_{24}Al_7X$. The corresponding experimental data [58, 59] and the calculated results [26] are shown in (a) and (b), respectively.

we calculated the electronic DOS and charge density difference (CDD) of the γ'-Ni_3Al phase. The phonon DOS was also calculated for alloys showing a pronounced alloying effect to obtain deeper insight into the elastic hardening mechanism of alloying.

5.1. Electronic structure

The total DOS of $Ni_{24}Al_7X$ (X = Al, Co, Re, and W) alloys are shown in figure 7. According to the results in the previous sections, $Ni_{24}Al_7X$ alloys with X = Co, Re, and W were chosen to elucidate the electronic origin of elastic hardening or softening due to alloying. From figure 7, alloying significantly alters the electronic DOS at the Fermi level. Compared with pure γ'-Ni_3Al, the Co-doped alloy has larger spectral weights at the Fermi level. In contrast, Re and W decreases the DOS at the Fermi level. According to the force theorem [60, 61], alloys with larger DOS at the Fermi level are more sensitive to elastic deformation of the crystalline lattice [62]. The total energy change (ΔE^{tot}) because of lattice distortion can be divided into two main parts: the kinetic energy change (ΔE^{ki}) and the change of electrostatic energy (ΔE^{es}) (i.e. $\Delta E^{tot} = \Delta E^{ki} + \Delta E^{es}$). The electrostatic term always has a positive contribution to the total energy change. However in response to the lattice deformation, the kinetic part (the leading term is the

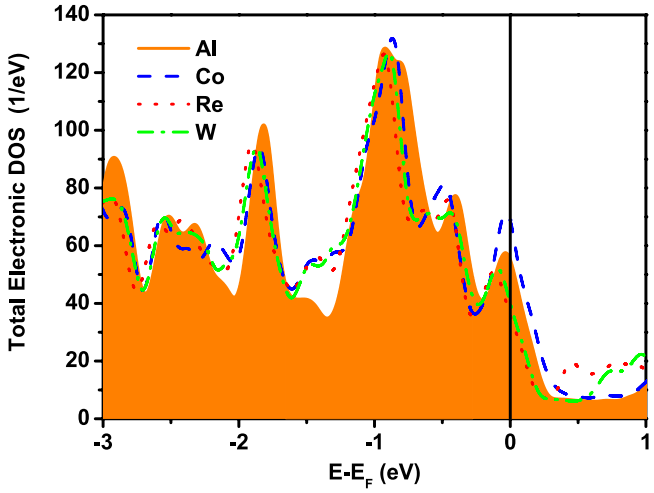

Figure 7. Total electronic DOS of $Ni_{24}Al_7X_y$ alloys with X = Al, Co, Re, and W. The Fermi level is shifted to zero.

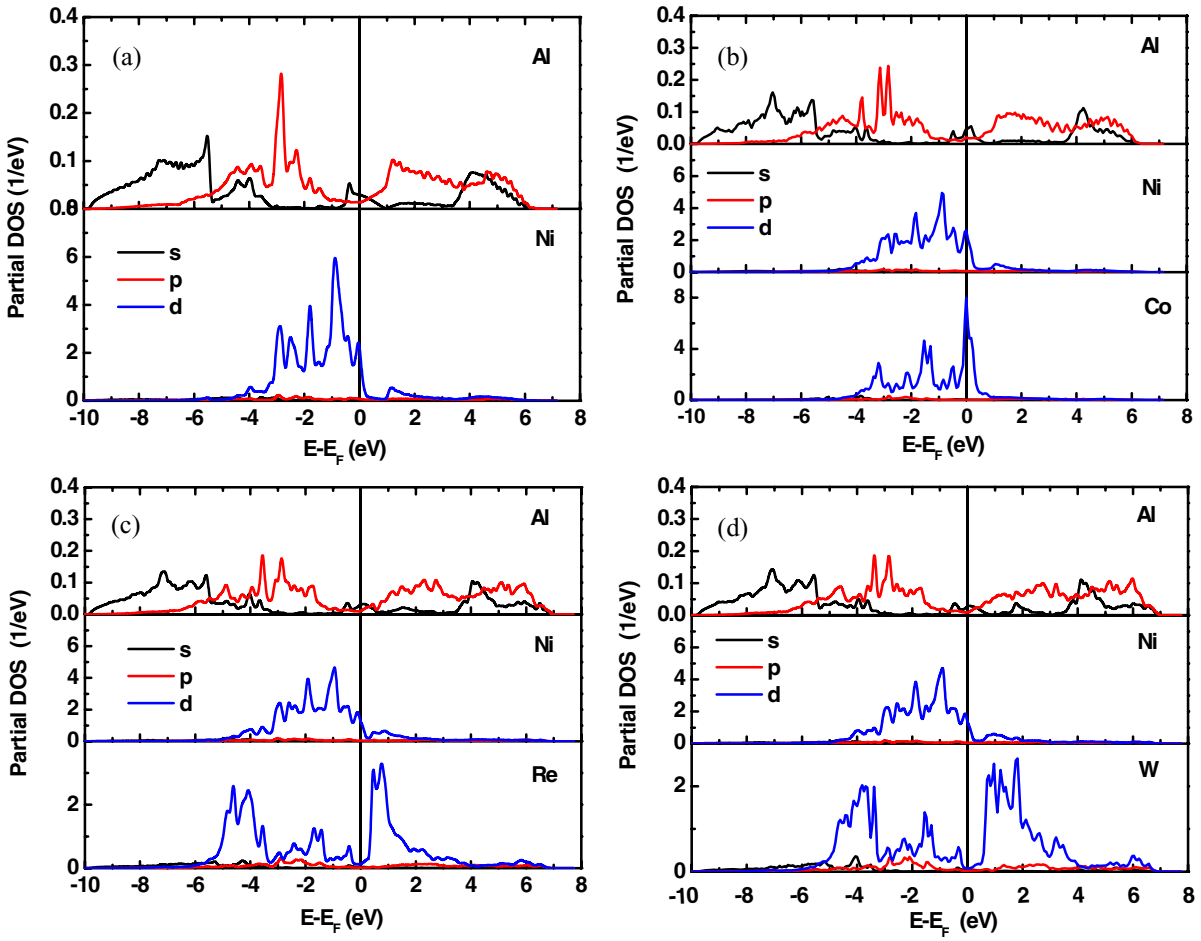

Figure 8. Partial electronic DOS of Al, Ni, and the alloying element X (X = Al, Co, Re, and W) in $Ni_{24}Al_7X$ alloys. The Fermi level is shifted to zero.

so-called one electron band energy [60]) has a negative contribution to the total energy, and this negative band energy is associated with the electronic DOS at the Fermi level. The larger DOS at the Fermi level contributes more negative band energy (in absolute value), resulting in a smaller change in total energy. Hence, the alloys that show a large DOS peak at the Fermi level (e.g. $Ni_{24}Al_7Co$) should have smaller shear moduli. Conversely, the alloys with a small DOS peak or a DOS valley at the Fermi level will be less sensitive to deformation, and will thus have larger elastic moduli. This simple scenario covers the self-consistent results obtained previously for $Ni_{24}Al_7X$ alloys. The alloying effect on the elastic behavior of the γ-Ni phase also follows this theoretical picture.

The partial electronic DOS of Ni, its first nearest neighbor (1NN) Al, and the 1NN X (X = Co, Re, and W) of Ni in the $Ni_{24}Al_7X$ alloys are plotted in figure 8. A few Al p electrons at the E_F level and broad overlap of the Al p and Ni d valence electrons from −6 to 0 eV indicates weak metallic bonding and strong covalent-like bonding between 1NN Ni–Al atoms in the γ'-Ni_3Al phases. The partial DOS of the Al and Ni atoms share an overlapping peak near −3 eV, which indicates hybridization of Al p and Ni d electrons. The Fermi level is located in the peak of the d electronic DOS of Co (see figure 8(b)), indicating metallic bonding between Co and the host Ni. In contrast, the Fermi level penetrates the pseudogap of the

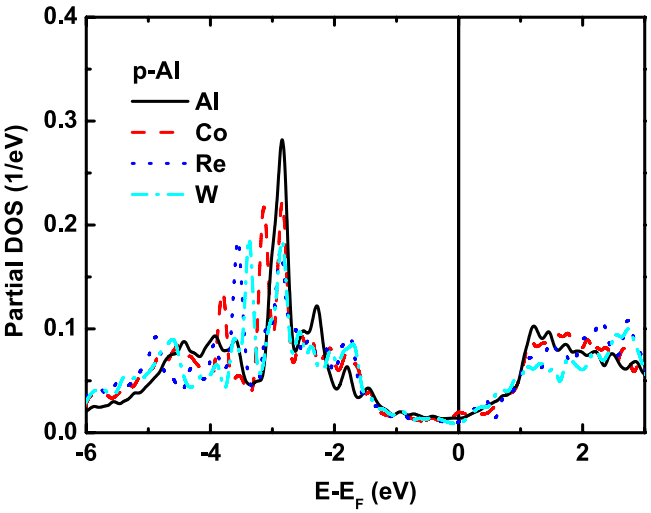

Figure 9. The p electronic DOS of the 1NN Al of the Ni atoms in the $Ni_{24}Al_7X$ alloys (X = Al, Co, Re, and W). The Fermi level is shifted to zero.

d band of Re and W (see figures 8(c) and (d)), which separates the bonding and anti-bonding states of the d-DOS of Re and W. This indicates that Re (W) and the host Ni atoms are more likely to form covalent-like bonding. Therefore, the alloying elements Re and W improve the mechanical properties of the

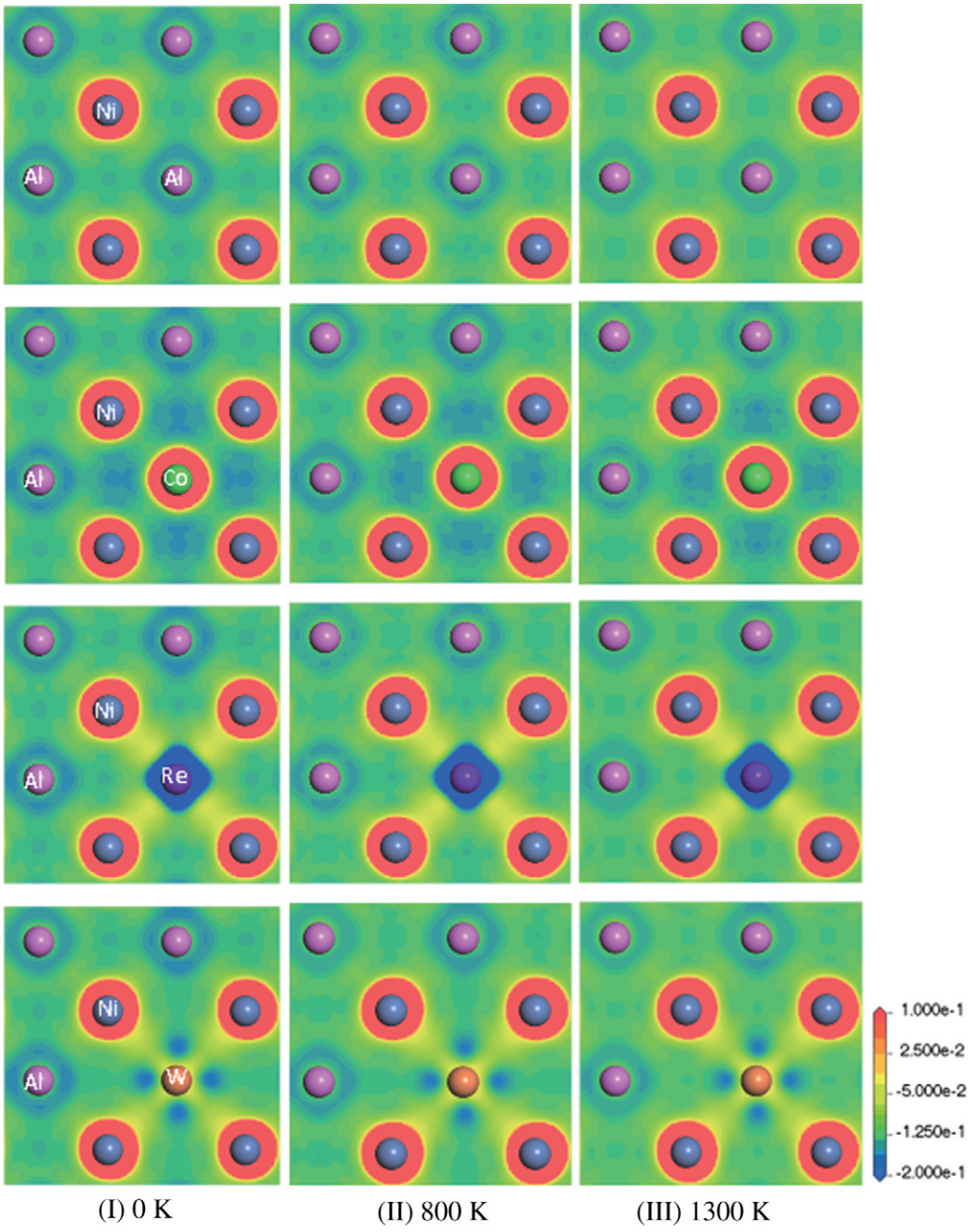

Figure 10. Charge density difference of $Ni_{24}Al_7X$ (X = Al, Co, Re, and W) on the (1 0 0) plane. The three columns represent the charge density differences at 0, 800, and 1300 K. The different colors of the spheres represent the different elements. Note that positive (negative) values denote the charge accumulation (depletion) in $e/(\text{a.u.})^3$.

Ni-based superalloys. In addition, to understand the interaction between the 1NN Al and X atoms around the Ni atom, the *p* electronic DOS of the Al atom (the same as in figure 8) in the different alloys are compared in figure 9. As can be seen from the figure that alloying splits the Al *p* electronic DOS peak at ~3 eV and push several states towards lower energy. Moreover, the pseudogap between two DOS peaks is the largest for the $Ni_{24}Al_7Re$ alloy and smallest for $Ni_{24}Al_7Co$. Comparing the DOS curves one can find that the *p* electronic states of Al in the $Ni_{24}Al_7X$ alloys shift to lower energy because of alloying. A simple estimate from integration of *p* DOS over the whole occupied states indicates that about ~0.002*e* additional charge per Al atom is observed for doped alloys. This means that alloying leads to charge transfer to Al atoms, and this additional *p*-band filling would stiffen the second nearest neighbor (2NN) Al–X bonding.

From the first column of the CDD (figure 10), an obvious directional distribution between Re (W) and NN Ni is observed. This indicates that the dopant Re and W form covalent-like bonding with the 1NN Ni atoms, resulting in larger shear elastic moduli. Co forms typical metallic bonds with the 1NN Ni atom, because charge accumulation around Co is nearly spherically symmetric. As a result, shear softening is observed in the $Ni_{24}Al_7Co$ alloy. These results are consistent

Table 3. Atomic charge (e) of Ni, Al, and X (X = Co, Re, and W) atoms for different doped alloys from Bader charge analysis.

Doped alloy	Atomic charge (e) from Bader charge analysis				
	Ni	Al	Co	Re	W
Ni_3Al	− 0.6007	1.8020	—	—	—
$Ni_{24}Al_7Co$	− 0.5359	1.8139	0.0542	—	—
$Ni_{24}Al_7Re$	− 0.5397	1.8298	—	0.2453	—
$Ni_{24}Al_7W$	− 0.5558	1.8152	—	—	0.6427

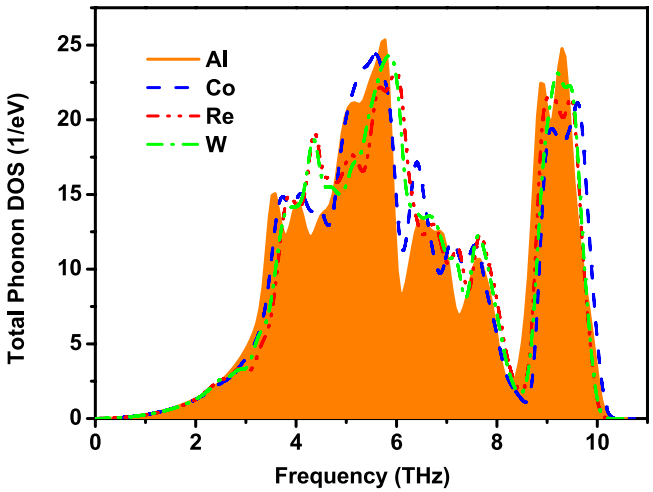

Figure 11. Total phonon DOS of $Ni_{24}Al_7X$ (X = Al, Co, Re, and W) alloys at 0 K.

with those discussed previously about DOS change because of alloying and the calculated self-consistent elastic constants. The temperature dependence of the thermophysical properties and elasticity can also be understood from the electronic structures. Comparing the CDD in the same row in figure 10, the charge distributions become increasingly sparse and uniform with increasing temperature because of increasing distance between the atoms for both the undoped and doped γ'-Ni_3Al phase. That is, the interactions between the atoms become weaker, which leads to elastic softening of the system with increasing temperature. Furthermore, the charge distribution features, such as Co showing metallic bonding and W and Re having covalent bonding features, always holds at high temperature (contour plots in the same row). Namely, the alloying effects are rather robust during temperature increase. This is in agreement with the temperature dependence of the elastic moduli, where Re and W always give larger c' and c_{44} in the temperature range considered.

A Bader charge analysis [63] was carried out for the obtained charge density of $Ni_{24}Al_7X$ (X = W, Re, and Co) alloys, and the results are shown in table 3. The atomic charges were obtained by subtracting the Bader charge from the number of valence electron considered for a particular atom in the DFT calculation. Doping has a pronounced effect on the local atomic charge. Compared with the charge at the Al site in the pure γ'-Ni_3Al phase, the positive atomic charges at the 2NN Al atom of X (Al atom of Ni_3Al) increase by 0.0432e, 0.0455e, and 0.0435e by adding W, Re, and Co into the γ'-phase, respectively. This suggests that the electrostatic interaction would increase. The negative charges at the 1NN Ni site of X atoms increase on average by ~0.0847e, ~0.1476e, and ~0.1567e for doping with W, Re, and Co in the γ'-phase, respectively. These findings are in agreement with the qualitative observations from both the partial DOS and CDD analysis.

5.2. Phonon spectra

The calculated total phonon DOS of $Ni_{24}Al_7X$ (X = Al, Co, Re, and W) alloys are plotted in figure 11. The orange curve (filled curve) shows the total phonon DOS of pure γ'-Ni_3Al. The localized modes of Re and W in the γ'-Ni_3Al phase are located at almost the same frequency. Two pronounced phonon DOS peak are observed at ~3.7 and ~4.3 THz for both the $Ni_{24}Al_7Re$ and $Ni_{24}Al_7W$ alloys. Three high DOS peaks located at ~5.3, ~6.2, and ~7.1 THz were found for Co in the γ'-Ni_3Al phase. The DOS peaks of Re and W at moderate frequency suggest that these alloys should have larger vibrational entropy than $Ni_{24}Al_7Co$. However, the Co-doped γ'-Ni_3Al phase has a large electronic DOS peak at the Fermi level, and the electron entropy overcomes the difference between the vibrational entropy of $Ni_{24}Al_7Co$ and $Ni_{24}Al_7W$, resulting in $Ni_{24}Al_7Co$ having the largest entropy at high temperature (see figure 4(d)).

A small stiffening of the phonon spectra is observed for the phonon DOS of the γ'-Ni_3Al phase doped with different elements. This is consistent with the calculated elastic moduli and electronic structure analysis. The high phonon DOS peak at high frequency (8.5–10 THz) is mainly because of the vibration of Al atoms. Alloying shifts the left margin (lower energy) of this DOS peak towards higher energy, indicating that addition of these elements strengthens the 2NN Al–X bonds. This is consistent with the partial electronic DOS analysis, which showed that p-band filling is the main contribution to 2NN stiffening. Comparing the effects of these three alloying elements, Co has the most pronounced effect. This is because Co forms nearly isotropic metallic bonds with neighboring atoms, and, consequently, the 2NN Al–Co interactions should be stronger than those of covalent-like bonding. The right shift of the right margin of the DOS peak at high frequency (~10 THz) is because of stiffening of the optical modes of Ni atoms, which is in agreement with the charge redistribution strengthening the 1NN Ni–X bond compared with the Ni–Al bond. The effect of alloying on the Ni–Ni 2NN bonding should be further analyzed through force constant calculations.

6. Summary

The influence of alloying elements X (X = Re, Ru, Ta, W, Mo, Cr, and Co) on the thermodynamic and elastic properties of the γ-Ni and γ'-Ni_3Al phases was systematically investigated by DFT. The quasiharmonic phonon approximation for volume expansion and the quasi-static approximation for elasticity were used in the calculations. The results show that alloying can effectively adjust the lattice misfit between the two phases, and Cr is a very important element for suppressing lattice misfit, and thus for improving

the creep resistance of alloys. The decrease in lattice misfit with temperature is because of the mismatch of the linear CTE between the two phases. We found that Ni_3Al has a small CTE and almost all of the alloying elements decrease its CTE. Therefore, the lattice misfit significantly decreases with increasing temperature. Thus, the improvement of the high-temperature creep strength of superalloys through the synergistic effect of co-doping is expected. The addition of alloying elements improves the incompressibility of both the γ-Ni and γ'-Ni_3Al phases, and the alloying elements Re and W have a pronounced effect. The refractory elements lead to tetragonal shear softening of the γ-Ni phase. For Ni–X alloys, Re, Ru, Cr, and Co slightly increase c_{44}, while Mo, W, and Ta decrease c_{44}. Importantly, alloying alters the temperature dependence of the elastic moduli. For example, Ru and Cr increase c', and Mo and W decrease c_{44} of the γ-Ni phase for $T > 900$ K. Namely, these elements are effective hardening elements for superalloys close to the working temperature. For the γ'-Ni_3Al phase, all of the alloying elements except Co considerably increase c' and c_{44} at finite temperature. Re and W atoms at Al sites were found to be most effective in hardening the γ'-Ni_3Al phase. Alloying does not considerably change the temperature dependence of the two cubic shear moduli. The calculated characteristics of superalloys can be understood by analysis of electronic structures and phonon spectra. It was found that the force theorem still holds in this superalloy system, and the electronic DOS details can account for the elastic hardening owing to alloying. Covalent-like bonding was found for Re and W with the 1NN Ni atoms, which accounts for the increased bulk modulus and two cubic shear moduli. Metallic-like bonding between Co and the neighboring atoms was found for the $Ni_{24}Al_7Co$ alloy, which is associated with the stiffening of the Al vibration mode. This shows that alloying not only strengthens the 1NN Ni–*X* bonding, but is also important for stiffening 2NN Al–*X* bonding. Thus, we speculate that doping of *d* metals into the γ'-Ni_3Al phase not only leads to additional *d*–*d* hybridization, but also increases the 2NN bonding through Al *p*-band filling.

Acknowledgments

This work was supported by the '973 Project' from the Ministry of Science and Technology of China (Grant No. 2011CB606402), the National Natural Science Foundation of China (Grant No. 51071091), and the Innovation Funds of Inner Mongolia University of Science and Technology (2010NC059). Authors are grateful to Prof Tao Yu and Dr Minru Wen for stimulating discussions. Simulations were performed using the 'Explorer 100' cluster system at the Tsinghua National Laboratory for Information Science and Technology, Beijing, China.

References

[1] Reed R C 2006 *The Superalloys Fundamentals and Applications* (New York: Cambridge University Press)

[2] Pollock T M and Tin S 2006 Nickel-based superalloys for advanced turbine engines: chemistry, microstructure, and properties *J. Propul. Power* **22** 361–74

[3] Bhadeshia H K D H 2003 Nickel based superalloys The website of University of Cambridge (www.msm.cam.ac.uk/phase-trans/2003/Superalloys/superalloys.html)

[4] Socrate S and Parks D M 1993 Numerical determination of the elastic driving force for directional coarsening in Ni-superalloys *Acta Metall. Mater.* **41** 2185–209

[5] Hazotte A, Bellet D, Ganghoffer J F, Denis S, Bastie P and Simon A 1992 On the contribution of internal mismatch stresses to the high-temperature broadening of gamma-ray diffraction peaks in a Ni-based single crystal *Phil. Mag. Lett.* **66** 189–96

[6] Yu X X and Wang C Y 2012 The effects of alloying elements on generalized stacking fault energies, strength and ductility of γ'-Ni3Al *Mater. Sci. Eng.* A **539** 38–41

[7] Yu X X, Wang C Y, Zhang X N, Yan P and Zhang Z 2014 Synergistic effect of rhenium and ruthenium in nickel-based single-crystal superalloys *J. Alloy Compd.* **582** 299–304

[8] Gülseren O and Cohen R E 2002 High-pressure thermoelasticity of body-centered-cubic tantalum *Phys. Rev.* B **65** 064103

[9] Kollie T G 1977 Measurement of the thermal-expansion coeffcient of nickel from 300 to 1000 K and determination of the power-law constants near the Curie temperatures *Phys. Rev.* B **16** 4872–81

[10] Rao P V M, Murthy K S, Suryanarayana S V and Naidu S V N 1993 High temperature thermal expansion characteristics of Ni3A1 alloys *J. Alloy Compd.* **190** L33–5

[11] Pavlovic A S, Babu V S and Seehra M S 1996 High-temperature thermal expansion of binary alloys of Ni with Cr, Mo and Re: a comparison with molecular dynamics simulations *J. Phys.: Condens. Matter* **8** 3139–49

[12] Taylor T A and Walsh P N 2004 Thermal expansion of MCrAlY alloys *Surf. Coat. Technol.* **177** 24–31

[13] Haynes J A, Pint B A, Porter W D and Wright I G 2004 Comparison of thermal expansion and oxidation behavior of various high-temperature coating materials and superalloys *Mater. High Temp.* **21** 87–94

[14] Barin I 1997 *Thermochemical Data of Pure Substances* (New York: Wiley-VCH)

[15] Amouyal Y, Mao Z G and Seidman D N 2010 Seidman effects of tantalum on the partitioning of tungsten between the γ- and γ'-phases in nickel-based superalloys: linking experimental and computational approaches original research article *Acta Mater.* **58** 5898–911

[16] Amouyal Y, Mao Z G and Seidman D N 2009 Phase partitioning and site-preference of hafnium in the γ'(L12)/γ(fcc) system in Ni-based superalloys: an atom-probe tomographic and first-principles study *Appl. Phys. Lett.* **95** 161909

[17] Fahrmann M, Hermann W, Fahrmann E, Boegli A, Pollock T M and Sockel H G 1999 Determination of matrix and precipitate elastic constants in (γ–γ') Ni-base model alloys, and their relevance to rafting *Mater. Sci. Eng.* A **260** 212–21

[18] Zhang X, Stoddart P R, Comins J D and Every A G 2001 High-temperature elastic properties of a nickel-based superalloy studied by surface Brillouin scattering *J. Phys.: Condens. Matter* **13** 2281–94

[19] Durst K, Franke O and Göken M 2004 Nanoindentations as a local probe for the mechanical properties and alloying influences in nickel-base superalloys and aluminide coatings ed K A Green *et al Superalloys Miner. Met. Mater. Soc.* 467–76

[20] Sieborger D, Knake H and Glatzel U 2001 Temperature dependence of the elastic moduli of the nickel-base superalloy CMSX-4 and its isolated phases *Mater. Sci. Eng.* A **298** 26–33

[21] Durst K and Göken M 2004 Micromechanical characterisation of the influence of rhenium on the mechanical properties in nickel-base superalloys *Mater. Sci. Eng.* A **387** 312–6

[22] Shang S L, Wang Y, Kim D E and Liu Z K 2010 First-principles thermodynamics from phonon and Debye model: application to Ni and Ni_3Al *Comput. Mater. Sci.* **47** 1040–8

[23] Shang S L, Kim D E, Zacherl C L, Wang Y, Du Y and Liu Z K 2012 Effects of alloying elements and temperature on the elastic properties of dilute Ni-base superalloys from first-principles calculations *J. Appl. Phys.* **112** 053515

[24] Kim D E, Shang S L and Liu Z K 2012 Effects of alloying elements on thermal expansions of γ-Ni and γ'-Ni_3Al by first-principles calculations *Acta Mater.* **60** 1846–56

[25] Wang Y, Liu Z K and Chen L Q 2004 Thermodynamic properties of Al, Ni, NiAl, and Ni_3Al from first-principles calculations *Acta Mater.* **52** 2665–71

[26] Wang Y, Wang J J, Zhang H, Manga V R, Shang S L, Chen L Q and Liu Z K 2010 A first-principles approach to finite temperature elastic constant *J. Phys.: Condens. Matter* **22** 225404

[27] Togo A, Chaput L, Tanaka I and Hug G 2010 First-principles phonon calculations of thermal expansion in Ti_3SiC_2, Ti_3AlC_2, and Ti_3GeC_2 *Phys. Rev.* B **81** 174301

[28] Parlinski K, Li Z Q and Kawazoe Y 1997 First-principles determination of the soft mode in cubic ZrO_2 *Phys. Rev. Lett.* **78** 4063–6

[29] Page Y L and Saxe P 2001 Symmetry-general least-squares extraction of elastic coefficients from *ab initio* total energy calculations *Phys. Rev.* B **63** 174103

[30] Wang Y J and Wang C Y 2009 Effect of alloying elements on the elastic properties of γ-Ni and γ'-Ni_3Al from first-principles calculations *MRS Fall Meeting Symp. FF Proc.*

[31] Wang Y J and Wang C Y 2009 First-principles calculations for the elastic properties of Ni-base model superalloys: Ni/Ni3Al multilayers *Chin. Phy.* B **18** 4339–48

[32] Wang Y J and Wang C Y 2009 Influence of the alloying elements on the elastic properties of the ternary and quaternary nickel-base superalloys *Phil. Mag.* **89** 2935–47

[33] Page Y L and Saxe P 2002 Symmetry-general least-squares extraction of elastic data for strained materials from *ab initio* calculations of stress *Phys. Rev.* B **65** 104104

[34] Shang S L, Sheng G, Wang Y, Chen L Q and Liu Z K 2009 Elastic properties of cubic and rhombohedral $BiFeO_3$ from first-principles calculations *Phys. Rev.* B **80** 052102

[35] Hamann D R, Wu X F, Rabe K M and Vanderbilt D 2005 Metric tensor formulation of strain in density-functional perturbation theory *Phys. Rev.* B **71** 035117

[36] Walker E and Bujard P 1980 Anomalous temperature behaviour of the shear elastic constant c_{44} in tantalum *Solid State Commun.* **34** 691–3

[37] Featherston F H and Neighbours J R 1963 Elastic constants of tantalum, tungsten and molybdenum *Phys. Rev.* **130** 1324–33

[38] Wang R, Wang S F, Wu X Z and Yao Y 2011 First-principles calculations on temperature-dependent elastic constants of rare-earth intermetallic compounds: YAg and YCu *Phys. B: Condens. Matter* **406** 3951–5

[39] Togo A, Oba F and Tanaka I 2008 First-principles calculations of the ferroelastic transition between rutile-type and $CaCl_2$-type SiO_2 at high pressures *Phys. Rev.* B **78** 134106

[40] Murnaghan F D 1944 The compressibility of media under extreme pressures *Proc. Natl Acad. Sci. USA* **30** 244–7

[41] Anderson O L and Isaak D G 1995 *Mineral Physics and Crystallography: A Handbook of Physical Constants* ed T J Ahrens (Washington D C: The American Geophysical Union) p 64

[42] Wasserman E F 1990 Moment-volume instabilities in transition metals and alloys *Ferromagnetic Materials* ed K H J Bushow and E P Wohlfarth vol 5 (Amsterdam: Elsevier) pp 237–322

[43] Davies G F 1974 Effective elastic moduli under hydrostatic stress --I. quasi-harmonic theory *J. Phys. Chem. Solids* **35** 1513–20

[44] Kresse G, Marsman M and Furthmüller J 2015 *VASP* manual: http://cms.mpi.univie.ac.at/vasp

[45] van de Walle A, Asta M and Ceder G 2002 The alloy-theoretic automated toolkit (ATAT): A user guide Calphad **26** 539–53

[46] Wang S Y, Wang C Y, Sun J H, Duan W H and Zhao D L 2001 Energetics and electronic structure of Re and Ta in the γ' phase of Ni-based superalloys *Phys. Rev.* B **65** 035101

[47] Zhou Y, Mao Z G, Booth-Morrison C and Seidman D N 2008 The partitioning and site preference of rhenium or ruthenium in model nickel-based superalloys: an atom-probe tomographic and first-principles study *Appl. Phys. Lett.* **93** 171905

[48] Blöchl P E 1994 Projector augmented-wave method *Phys. Rev.* B **50** 17953–79

[49] Kresse G and Joubert D 1999 From ultrasoft pseudopotentials to the projector augmented-wave method *Phys. Rev.* B **59** 1758–75

[50] Perdew J P, Burke K and Ernzerhof M 1996 Generalized gradient approximation made simple *Phys. Rev. Lett.* **77** 3865–8

[51] Methfessel M and Paxton A T 1989 High-precision sampling for Brillouin-zone integration in metals *Phys. Rev.* B **40** 3616–21

[52] Monkhorst H J and Pack J D 1976 Special points for Brillouin-zone intergrations *Phys. Rev.* B **13** 5188–92

[53] De Boer F R, Schinkel C J, Biesterbos J and Proost S 1969 Exchange-enhanced paramagnetism and weak ferromagnetism in the Ni_3Al and Ni_3Ga phases; giant moment inducement in Fe doped Ni_3Ga *J. Appl. Phys.* **40** 1049–55

[54] Ruban A V and Skriver H L 1997 Calculated site substitution in ternary γ'-Ni3Al: temperature and composition effects *Phys. Rev.* B **55** 856–74

[55] Stoloff N S 1972 *The Superalloys* ed C T Sims and Hagel W C (New York: Wiley) p 103

[56] Touloukian Y S and Ho C Y 1989 *Properties of Selected Ferrous Alloying Elements* (New York: Hemisphere)

[57] Shang S L, Saal J E, Mei Z G, Wang Y and Liu Z K 2010 Magnetic thermodynamics of fcc Ni from first-principles partition function approach *J. Appl. Phys.* **108** 123514

[58] Tanaka K and Koiwa M 1996 Single-crystal elastic constants of intermetallic compounds *Intermetallics* **4** S29–39

[59] Prikhodko S V, Carnes J D, Isaak D G, Yang H and Ardell A J 1999 Temperature and composition dependence of the elastic constants of Ni3Al *Metall. Mater. Trans.* A **30** 2403-8

[60] Skriver H L 1985 Crystal-structure from one-electron theory *Phys. Rev.* B **31** 1909–23

[61] Mackintosh A R and Andersen O K 1980 *Electrons at the Fermi Surface* (Cambridge: Cambridge University Press)

[62] Zhang H L, Punkkinen M P J, Johansson B, Hertzman S and Vitos L 2010 Temperature and composition dependence of the elastic constants of Ni_3Al *Phys. Rev.* B **81** 184105

[63] Bader R F 1990 *Atoms in molecules-A Quantum Theory* (Oxford: Oxford University Press)